Title

Proteolysis of Amyloid β by Lysosomal Enzymes as a Function of Fibril Morphology

Journal

ACS Omega, 6(47)

ISSN

2470-1343

Authors

Lambeth, Tyler R

Julian, Ryan R

Publication Date

2021-11-30

DOI

10.1021/acsomega.1c03915

Peer reviewed

ACS OMEGA

http://pubs.acs.org/journal/acsodf

Article

Proteolysis of Amyloid β by Lysosomal Enzymes as a Function of Fibril Morphology

Tyler R. Lambeth and Ryan R. Julian*

Cite This: *ACS Omega* 2021, 6, 31520−31527

Read Online

ACCESS | Metrics & More | Article Recommendations | Supporting Information

ABSTRACT: Aggregation of amyloid-β (Aβ) into extracellular plaques is a well-known hallmark of Alzheimer's disease (AD). Similarly, autophagic vacuoles, autophagosomes, and other residual bodies within dystrophic neurites, though more difficult to detect, are characteristic features of AD. To explore the potential intersection between these observations, we conducted experiments to assess whether Aβ fibril formation disrupts proteolysis by lysosomal enzymes. Fibrils constituted by either Aβ 1−40 or Aβ 1−42 were grown under both neutral and acidic pH. The extent of proteolysis by individual cathepsins (L, D, B, and H) was monitored by both thioflavin T fluorescence and liquid chromatography combined with mass spectrometry. The results show that all Aβ fibril morphologies are resistant to cathepsin digestion, with significant amounts of the undigested material remaining for samples grown in either neutral or acidic pH. Further analysis revealed that the neutral-grown fibrils are proteolytically resistant throughout the sequence, while the acid-grown fibrils prevented digestion primarily in the C-terminal portion of the sequence. Fibrils grown from Aβ 1−42 are generally more resistant to degradation compared to Aβ 1−40. Overall, the results indicate that Aβ fibrils formed in the neutral pH environments found in intracellular or extracellular spaces may pose the greatest difficulty for complete digestion by the lysosome, particularly when the fibrils are comprised of Aβ 1−42.

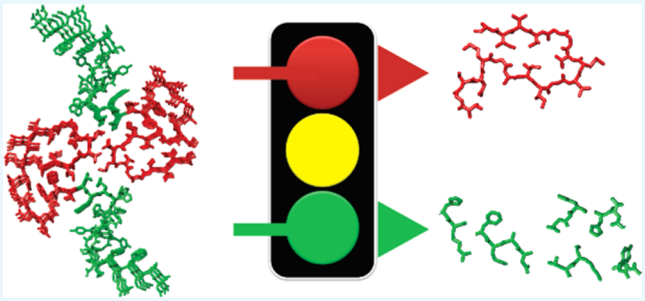

INTRODUCTION

Autophagy is a critical process needed to clear cellular waste and free up resources for reuse or energy production. Within this framework, autophagy delivers peptides and proteins to the lysosome where they are digested into constituent amino acids, forming a crucial cog in the gears that drive proteostasis.[1] Target substrates can be gathered from inside the cell or from the extracellular space through endocytosis.[2] Due to a variety of pathways leading to the lysosome, substrates can be subjected to many conditions and environments prior to fusion with a lysosome. Additionally, the endo/lysosomal system utilizes acidic compartments for the delivery and degradation of substrates, further expanding the range of different environments that may be experienced prior to degradation.[3] Failure of the endo/lysosomal system can lead to a variety of complications, including a class of diseases known as lysosomal storage disorders. Lysosomal storage is most frequently caused by hydrolase dysfunction, which leads to the accumulation of undigested substrates and eventual failure of the organelle.[4] Autophagic disruption has also been associated with Alzheimer's disease (AD) due to the hallmark observation of lysosomal storage.[5,6] Endosome abnormality is one of the earliest features observed in an AD brain, and further connections have been drawn between known pathological mutations in presenilin 1 and 2, which play roles in lysosomal acidification and clearance.[7] As Amyloid β (Aβ) can be produced by proteolytic cleavage in late endosomes by β-secratase-1, dysfunction of this system can also lead to accumulation of Aβ fibrils in lysosomes.[8]

Inside the lysosome, hydrolases known as cathepsins degrade peptides and proteins into the constituent amino acids, which are then released by transporter proteins back into the cytosol.[9] While a few members of the cathepsin family are exopeptidases, which cleave from the termini, the majority are endopeptidases, which cleave somewhere in the middle of the sequence.[10] Among the endopeptidases, the most abundant and active are cathepsin L (catL, all cathepsins will be abbreviated similarly) and catD.[11] Studies have demonstrated that knocking out either catD or catL induces pathology and death in mice within 4 weeks.[12,13] The most abundant lysosomal exopeptidase, catB, recognizes and binds to the C-terminus (as well as the C-terminal mimic L-isoAsp)[14] and removes two amino acids at a time as dipeptides. The complementary aminopeptidase, catH, works from the N-

Received: July 22, 2021
Accepted: November 8, 2021
Published: November 18, 2021

https://doi.org/10.1021/acsomega.1c03915
ACS Omega 2021, 6, 31520−31527

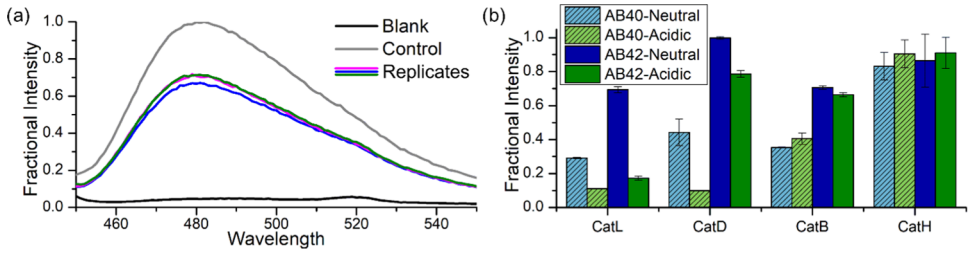

Figure 1. (a) Three replicates for ThT fluorescence following digestion of Aβ42-Neutral by catL. (b) Compiled fluorescence data for all cathepsin incubations. The dark blue peak for CatL derived from the data in (a).

terminus to remove one amino acid at a time. Although catB and catH are primarily exopeptidases, they both possess secondary endopeptidase activity.[15,16] Knockouts of catB also cause shortened lifespans,[10] while knockouts of catH lead to significantly reduced levels of important neurotransmitter peptides.[17] These studies demonstrate that while the cathepsins perform similar functions, each enzyme is individually vital to maintain proteostasis.

Amyloid β (Aβ) is a peptide of typically 39−42 residues known to aggregate into fibrils,[18] similar to other amyloid proteins such as human islet amyloid polypeptide[19] and CsgA.[20] As the target of autophagy, Aβ (including fibrils), can be trafficked from both intracellular and extracellular spaces to the lysosome.[21] One method of extracellular Aβ clearance involves internalization by astrocytes.[22] Oligomeric and fibrillar forms can be transferred to astrocytic lysosomes for degradation, with oligomeric forms being removed at a higher rate. Aβ fibrils have been shown to impede digestion by proteases such as trypsin[23] and bovine brain proteases.[24] In a related system, α-synuclein aggregates were found to resist degradation by catL.[25] These previous experiments suggest that amyloid fibrils are resistant in varying degrees to degradation by proteases. Aβ spontaneously assembles into fibril structures in solution via side chain and backbone interactions. Aβ fibrils are comprised primarily of stacked β-sheet structures stabilized by hydrophobic interactions along the middle and C-terminal regions of the sequence.[26,27] Additionally, Aβ fibrils are often polymorphic and comprised of strands that vary in the molecular arrangement of constituent peptides.[28,29] NMR experiments have shown that accessible morphologies include β sheet layers composed of dimeric or trimer assemblies of Aβ.[30−32] Notably for both of these morphologies, the β-sheet core remains tightly bound, while the N-terminal residues from 1 to 14 are disordered. Fibril formation is affected by a number of environmental conditions. Increasing the solution ionic strength can accelerate aggregation rates while favoring formation of a more stable fibril form.[33] Mutations in the sequence such as the Tottori (D7N) and English (H6R) mutations produce higher-order oligomers with more β-strand structure, resulting in higher toxicity for cultured neuronal cells.[34] The Tottori and Iowa (D23N) mutations additionally introduce the possibility of deamidation, which generates aspartic acid isomers and enhances aggregation propensity and toxicity.[35]

The pH during fibril formation also impacts fibril morphology. For example, fibrils formed in acidic environments differ from those formed at neutral pH and time course measurements of fibril formation show that aggregation occurs faster at lower pH.[36] Importantly, acidic conditions present in the lysosome could facilitate alternate morphologies for fibrils formed therein.[37] The structural difference caused by lower pH is attributed to varying protonation states of histidine residues in the sequence.[38] While other ionizable groups are unaffected by a shift from cellular to lysosomal pH, the pK_a value for the imidazole group comprising the side chain of histidine lies in the middle of the relevant pH range. As a consequence, histidine is likely to become protonated in acidic compartments. The formation of amyloid β fibrils is driven by hydrophobic interactions between the peptide chains and as such can potentially be altered by hydrophilic charges.[39] The resulting differences between fibrils due to His protonation were observed using transmission electron microscopy, revealing markedly different morphology distributions.[40] By substituting alanine for histidine residues, it was then demonstrated that protonation of side chains for His6, His13, and His14 significantly affects fibril structure by disfavoring amyloid sheets in the N-terminal half of the sequence. The effect of protonation on morphology is further evidenced by the changes seen in the English (H6R) mutation.[34] In the body, the majority of Aβ is located extracellularly; however, it is known to accumulate in the lysosome of neuronal cells during the process of autophagy.[37] Monomeric Aβ trafficked in acidic environments of the lysosomal system would fibrilize under different conditions than the extracellular space. Due to the origination of fibrils in neutral and acidic cellular spaces, fibrils with varied morphologies could be delivered to the lysosome, distinctly affecting the interactions with cathepsin proteases.

Herein, we examine incubations of fibrils grown at cellular and acidic pH with lysosomal cathepsins to evaluate their ability to degrade these structures. Analysis was performed via thioflavin T (ThT) fluorescence to measure the general extent of degradation, and proteolytic products were also quantitatively assessed with liquid chromatography/mass spectrometry (LC−MS). Significant differences were observed in the amount of degradation as a function of the pH used to grow the fibrils and whether the fibrils were composed of Aβ40 or Aβ42. Further examination of these digestions with mass spectrometry revealed differences in both the identified sequences and length of peptides remaining after incubation. By plotting these products as a function of intensity, we were able to map proteolytically resistant regions as a function of fibril composition and pH during formation.

RESULTS AND DISCUSSION

Amyloid β 1−40 (Aβ40) and 1−42 (Aβ42) were incubated at pH 5 and pH 7.2 to produce stable fibrils with varying morphologies. Importantly, fibrils formed at different pH do not interconvert if the pH is shifted after fibrils have formed.[41] These fibrils were then digested over an 18 h period in separate experiments by cathepsin L, D, B, and H, which represent two crucial endopeptidases, one carboxypeptidase, and one amino-

https://doi.org/10.1021/acsomega.1c03915
ACS Omega 2021, 6, 31520−31527

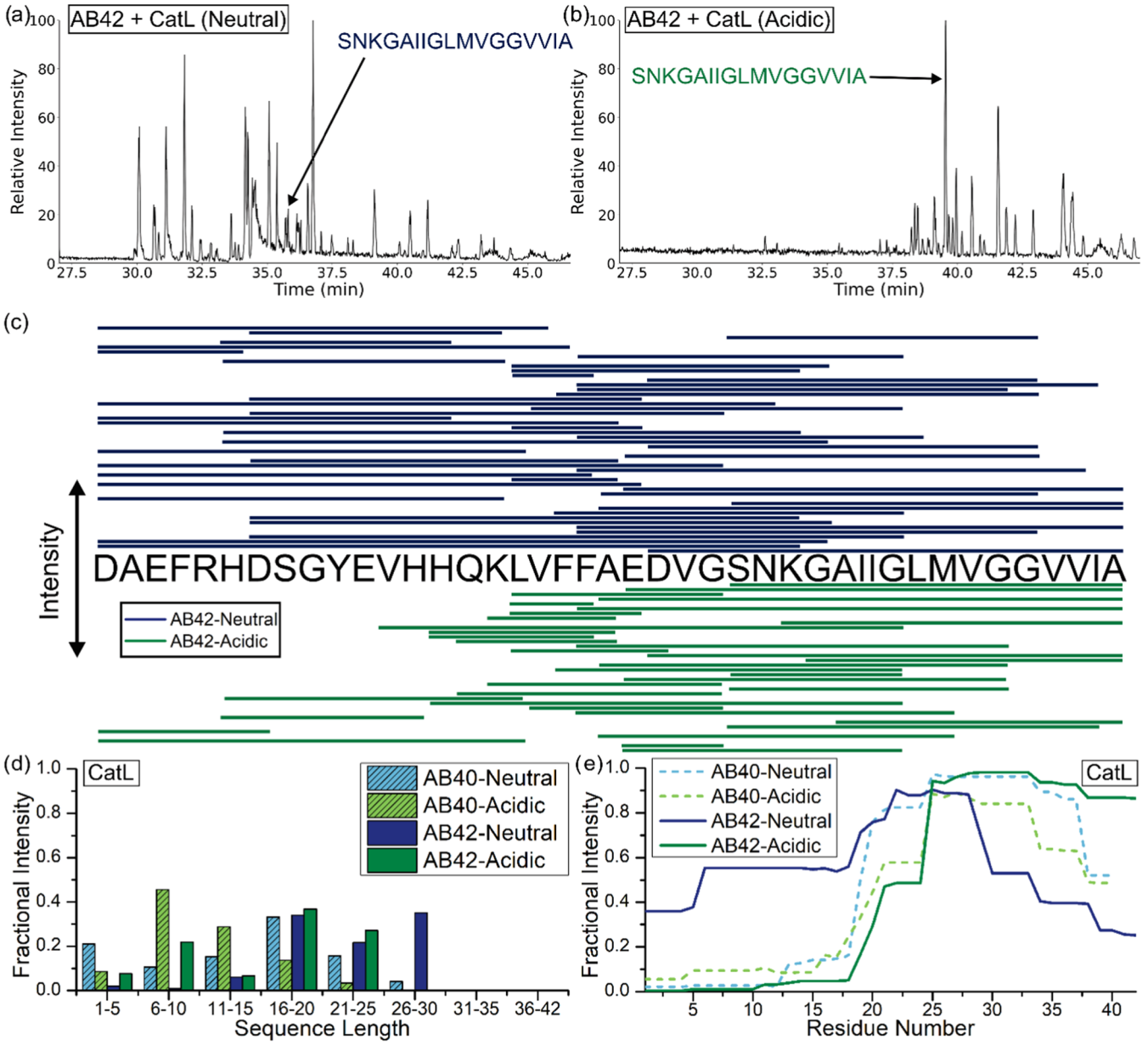

Figure 2. (a) Raw chromatogram for the digestion of Aβ42-neutral and (b) Aβ42-acidic by catL. The proteolytic product Aβ 16−42 is shown in both chromatograms as a reference. (c) Compiled line diagram of the identified peptides from the chromatograms. Lines indicate which part of the full sequence comprises the proteolytic product. Products are ordered by intensity, with the most intense products listed closer to the full sequence. (d) Bar plot showing the length of the identified product peptides. (e) Plot of the residue intensity among the total intensity of all peptides with a length greater than 10, representing areas resistant to proteolysis.

peptidase. Although the pH was varied to create fibrils with differing morphology, the digestion experiments for both types of fibrils were conducted at identical pH corresponding to the optimal value for each cathepsin. The extent of digestion was coarsely measured by ThT fluorescence intensity, as shown in Figure 1a for the digestion of neutral Aβ42 by catL. ThT is a fluorescent dye used to measure the presence of protein and peptide aggregates due to its ability to fluoresce intensely when bound to β-sheet-rich structures.[42] The fractional intensity of fluorescence remaining after digestion represents the amount of remaining β-sheet-rich structures present in the sample after proteolysis. The fluorescence data from all cathepsin digestions are compiled in Figure 1b. For the endopeptidases, catL digested more fibril relative to catD. For the acid-grown fibrils (in green), catL reduced the amount of fluorescence by >80% from the initial level. However, for the neutral-grown fibrils less digestion was observed, particularly for Aβ42, which only exhibited a ∼30% reduction in fluorescence intensity. Similarly, catD reduced ThT fluorescence less for neutral-grown fibrils less and yielded almost no change for the neutral Aβ42 fibrils.

Endopeptidases operate by binding to several amino acids on either side of the peptide bond targeted for hydrolysis and as such are potentially sensitive to differences in substrate backbone structure in either direction of the surrounding sequence region. In contrast, catB and catH act primarily as exopeptidases and have the strongest interactions with residues to one side of the targeted peptide bond. For catH, digestion of Aβ42 and Aβ40 yielded similar results and reductions in ThT fluorescence were not significant for either acidic or neutral fibrils. This suggests that catH was unable to access the

https://doi.org/10.1021/acsomega.1c03915
ACS Omega 2021, 6, 31520−31527

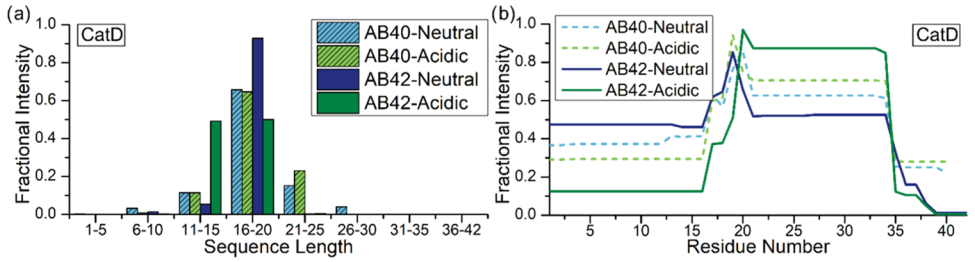

Figure 3. (a) Bar plot of the sequence length of identified proteolytic products from catD incubations. (b) Plot of the residue intensity among the total intensity of all peptides with a length greater than 10.

amyloid region lending ThT fluorescence, although it is unclear whether any portion of the N-terminus was digested. For catB, which attacks from the C-terminal side, significantly more ThT fluorescence was retained by the Aβ42 fibrils for both acidic and neutral fibers. Indeed, neutral or acidic conditions had little effect on the catB results, suggesting that differences in fibril structure likely occur near the N-terminus (as discussed in the introduction section). Although there are clear differences in the ThT results for our various test conditions, more detailed information would likely facilitate greater understanding.

To more precisely determine the outcome of each cathepsin digestion, the samples were analyzed with a combination of liquid chromatography and mass spectrometry. These experiments were able to identify the precise peptides remaining following proteolysis and defibrilization. Since fibrils inhibit complete degradation, the surviving peptides yield structural information about undigested regions similar to experiments employing limited proteolysis.[43] Raw chromatograms of the digestion of Aβ42 with catL are shown in Figure 2a,b for neutral and acidic fibrils, respectively. Notable differences in retention times and relative intensities are apparent, suggesting that the two experiments generated considerably different peptide profiles. This possibility is confirmed by MS analysis, which is illustrated schematically in Figure 2c. Each identified sequence from the chromatograms in Figure 2a/b is displayed as an individual line in Figure 2c, where the length of each line maps out the corresponding peptide sequence in relation to the full sequence shown in the middle of the diagram. Peptide identifications were made using CID fragmentation data, as demonstrated in Figure S1. The sequences are also ordered by intensity, with more intense peptides displayed closer to the full Aβ42 sequence. The full list of peptides can also be found in Tables S1 and S2 in the Supporting Information. Peptides located in the C-terminal portion of Aβ42 were found for both acidic and neutral fibrils, indicating resistance to catL digestion in this region. However, for the neutral fibrils, a variety of peptides were found from the N-terminal region, including many peptides that contained the N-terminus itself. These results suggest that the amyloid-forming region is resistant to digestion for both acidic and neutral fibrils, but that the N-terminal region is accessible and susceptible to digestion for acidic fibrils. The data from Figure 2c can be more succinctly summarized with additional analysis, as shown in Figure 2d,e. In Figure 2d, histograms of residual peptide length are shown for four different experiments: neutral Aβ40, acidic Aβ40, neutral Aβ42, and acidic Aβ42. Aβ42 digestion products skew more toward the longer sequence lengths in general, while Aβ40 digestion products are clustered in smaller length peptides. Notably, the 26−30 length bin contains only intensity from neutral-grown fibrils of Aβ40 and Aβ42. When compared to the catL digestion of monomeric Aβ42 collected in Table S3 and displayed as histograms in Figure S2, a striking difference is observed. In the monomeric digest, nearly 80% of the peptide products are of lengths less than 5 amino acids long, and there are no peptides observed greater than 15 residues long. This contrast in peptide lengths demonstrates a substantial obstruction is occurring in the proteolysis of Aβ fibrils. It is also possible that some amount of protofibrils or other oligomeric forms may be present in our samples, reflecting the heterogeneity typical of such experiments. However, the data illustrate that large undigested portions remain in all samples compared to homogenous monomeric digests, and differences between samples are notable in every case.

Proteolysis experiments may proceed in a stepwise manner leading to accessibility for some previously blocked regions after initial cleavages; however, the longest sequences represent lasting resistance throughout the course of the digestion. To visually display a summary of the regions with the most resistance to proteolysis, sequences with a length of at least 11 amino acids were used to generate an intensity map, as shown in Figure 2e. The fractional intensity value (y-axis) for each residue (x-axis) was calculated by adding up the intensity of all peptides containing the residue and then dividing by the intensity of all peptides. Only peptides longer than 11 residues were included. Accordingly, a fractional intensity value of 0.5 means that the residue is present in 50% of the total peptide intensity that was observed. It should be noted that peptide intensity is influenced by many factors including the number of acidic, basic, and hydrophobic amino acids and does not correlate precisely with concentration.[44,45] Therefore, the plot in Figure 2e should not be interpreted to represent absolute quantitation but rather a semiquantitative evaluation that is most meaningful when comparing relative abundances for differing fibrils for which the intensity at each amino acid will be based on the intensities of peptides with very similar (or identical) sequences. Examination of the solid lines (derived from Aβ42 data) reveals excellent agreement with the representation shown in Figure 2c. Again, differences in product profiles between various digestions are apparent. The C-terminal region is resistant to proteolysis in all cases. Interestingly, neutral Aβ42 fibrils are the most resistant in the N-terminal region. For Aβ40, less difference is noted between digestion of acidic and neutral fibrils. These results are consistent with the fluorescence data shown in Figure 1b, where the neutral-grown fibrils display a higher amount of intensity after digestion in both Aβ40 and Aβ42, demonstrating an increase in proteolytic resistance.

https://doi.org/10.1021/acsomega.1c03915
ACS Omega 2021, 6, 31520−31527

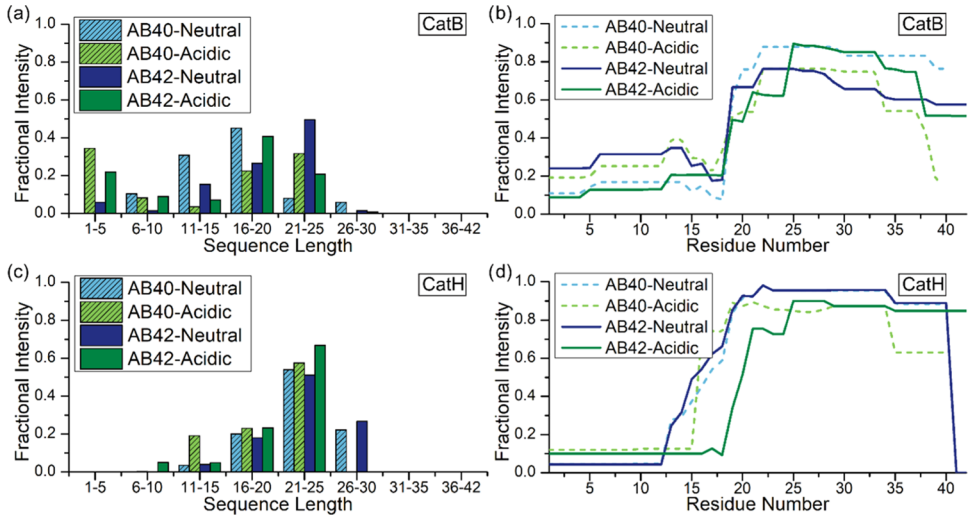

Figure 4. (a) Bar plot of the sequence length of identified proteolytic products from exopeptidase catB incubations and (c) catH incubations. (b) Plot of the residue intensity among the total intensity of all peptides with a length greater than 10 for catB incubations and (d) catH incubations.

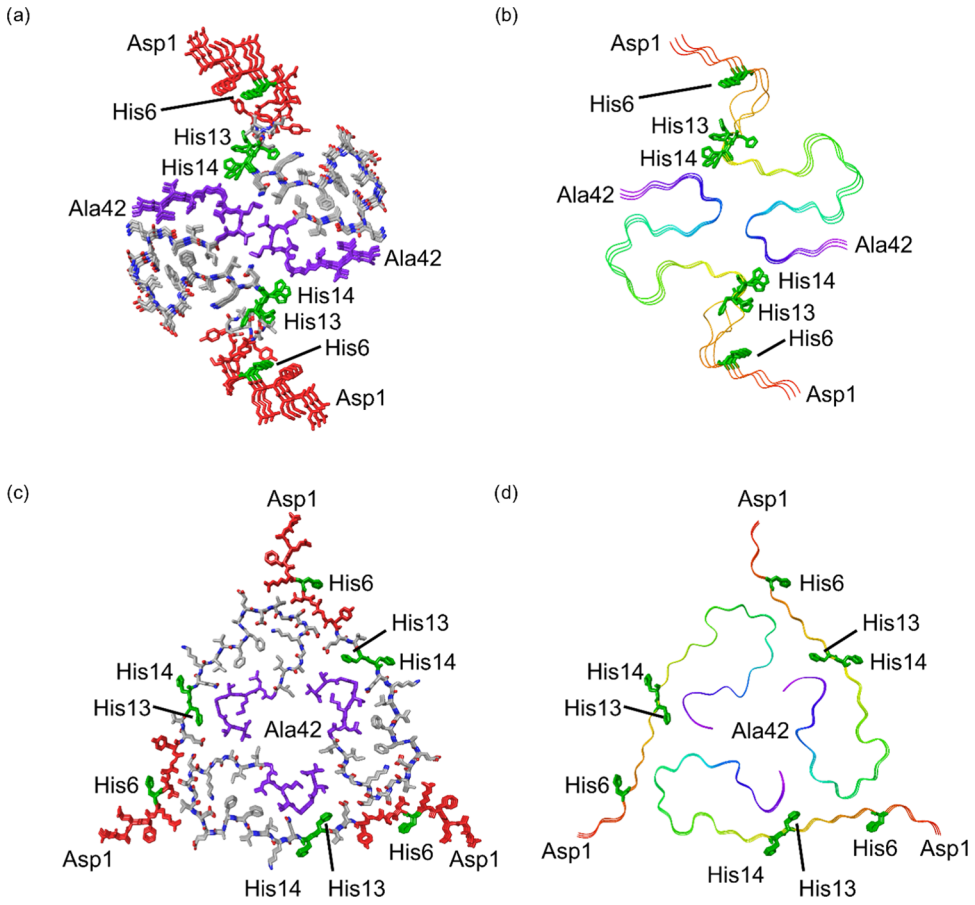

Figure 5. (a) Tube representation and (b) ribbon representation of the Aβ 1−42 dimer fibril (PDB: 2NAO). The N-terminal region is shown by highlighting residues 1−10 in red and protrudes in a disordered fashion from the fibril core. The C-terminal region is shown by highlighting residues 33−40/42 in purple with the exposed tail sticking out from the hydrophobic core. Relevant histidine residues are shown in green. (c) Tube representation and (d) ribbon representation of the Aβ 1−40 trimer fibril (PDB: 2M4J). The N-terminal region is exposed with some accessibility of the following residues until the bend region.

The same analysis was performed on digestions with the endopeptidase catD, as shown in Figure 3. The peptide lengths shown in Figure 3a consist of a tighter spread than those seen with catL digestions. Interestingly, the neutral-grown Aβ42 products are almost entirely sequences with lengths of 16−20 residues. Although most of the intensity from Aβ40 digestions is found in the 16−20 length as well, some peptides were also identified with lengths greater than 20. The absence of shorter peptides may suggest that fewer acceptable binding sites exist for catD or that it is less capable of digesting fibrils in general.

https://doi.org/10.1021/acsomega.1c03915
ACS Omega 2021, 6, 31520−31527

The catD digestion of the monomeric Aβ42 is illustrated in Table S4 and displayed in Figure S3. The distribution of intensities suggests that catD is able to more easily bind and degrade sequences in the monomer form, populating the 6−10 and 11−15 bins with around 65% of the product intensity. Additionally, the 1−5 length bin contains a small portion of the intensity, while none is present in either Aβ42 fibril digestion. The peptide intensity map shown in Figure 3b reveals some similar trends to the previous catL digestions. All digestions showed a resistant region in the C-terminal half of the sequence, extending from around Lys16 to Met35. In the neutral-grown Aβ42, nearly half of the peptides originating from the N-terminal half of the sequence survive digestion. The Aβ40 digests for both acidic and neutral fibrils also yielded more N-terminal peptide intensity. The fluorescence data for these samples shown in Figure 1b is higher for both digestions of neutral-grown Aβ, which indicates that the resistant residues in the N-terminal half may be contributing to the formation of greater amounts of stacked β-sheet content involved in ThT binding.

Identical analyses for results from catB and catH are shown in Figure 4. These enzymes act primarily as exopeptidases, though both possess some endopeptidase activity. Examining the data for the catB digests in Figure 4a reveals a wide spread of peptide lengths. The Aβ42-neutral fibril distribution is skewed toward longer lengths, while the Aβ40 neutral fibrils are distributed more toward the center of the distribution. Acidic fibrils from both Aβs populate bimodal distributions, favoring longer and shorter peptides. The peptide intensity map is shown in Figure 4b. Although catB is a carboxypeptidase, which cleaves from the C-terminus, it is unable to progress very far before encountering resistance. Indeed, only the acidic fibrils from Aβ40 reveal any cleavage at the C-terminus that is nearly complete. Ironically, most of the degradation for catB takes place due to secondary endopeptidase activity in the N-terminal region.

In the length histograms for catH shown in Figure 4c, the majority of all peptide intensity is observed in peptides of length 21−25. CatH is an aminopeptidase that preferentially cleaves one amino acid at a time and is likely to produce products that will not be retained by LC. Notably, peptides of the longest observed length (26−30) were only recorded for the neutral-grown fibrils. In the residue intensity plot for catH shown in Figure 4d, the N-terminal region is similarly digested for all four experiments. The primary differences in Figure 4d relate to Aβ42. The acidic fibrils allow greater penetration in the N-terminal region, while an unexpected cleavage at the C-terminus is observed for the neutral fibrils. This C-terminal cleavage goes essentially to completion as with the catD digests and is more efficient than the C-terminal cleavage observed for catB. The smaller differences between these digestion profiles are similarly reflected in the smaller differences between the fluorescence intensity shown in Figure 1b.

Two commonly observed fibril morphologies for both Aβ40/42 are comprised of either dimeric layers (PDB: 2NAO) or trimeric layers (PDB: 2M4J) of β sheets, as shown in Figure 5. In the dimer form, the N-terminal region is a disordered strand that extrudes from the fibril core. This morphology exposes the N-terminus and is consistent with the high digestion levels that we observed for all cathepsins. In particular, little resistance was encountered in the N-terminal region for catH, although the acidic fibrils appear to have greater exposure, particularly for Aβ42. His13 and His14 bridge the transition between the N-terminal tail and the more organized β-sheet. When protonated, the hydrophilic side chains of His may lead to additional disorder. Additionally, the C-terminal tail is exposed for the dimeric fibril, making it easier for the cathepsins to cleave (as is observed in almost all of the cathepsin incubations). The digestion results match the expected protection afforded by the dimeric structure rather well, suggesting that a significant fraction of the fibrils present in our digestion may be comprised of similar dimeric sheets.

In the trimeric form, the N-terminal region is ordered but still represents the most solvent-exposed region of the peptide, protecting the β sheet and the C-terminus that are obscured with the core. This structure would be more easily digested near the N-terminus as well, and protonated histidine side chains would also contribute to looser binding and more solvent exposure in the acid-grown fibril samples. This structure would be less available for enzymatic binding as it nears the bend region from residues 19−28, which is consistent with the sloped increase of residue intensity observed for all cathepsin incubations in the same region. However, the buried C-terminal tail would be expected to make digestion difficult from this side of the peptide. Given that we observe digestion of C-terminal residues, particularly for catD, this morphology is not likely the dominant in form present in our fibrils.

CONCLUSIONS

We have examined the influence of fibril formation on the proteolysis of both Aβ40 and Aβ42 in a detailed and quantitative fashion. It is clear that fibril formation interferes with proteolysis by the major lysosomal cathepsins in every case. The differential digestion obtained for fibrils formed at either neutral or acidic pH confirms the likelihood that such fibrils have distinct structures, mostly related to the N-terminal portion of the sequence. Overall, our results suggest that fibrils composed of Aβ42 and formed at neutral pH will present the greatest difficulty for digestion within the lysosome. In contrast, the monomeric Aβ is easily digested by cathepsins and appears unlikely to contribute to lysosomal pathology. However, our results suggest that it is possible for amyloid fibrils to contribute to AD pathology and the lysosomal storage observed in the disease by simply evading degradation.

EXPERIMENTAL PROCEDURES

Fibril Formation. Lyophilized Aβ powder was purchased from Anaspec. The samples were disentangled via ammonium hydroxide treatment.[46] One hundred micrograms aliquots of each peptide were dissolved in 50 μL of 0.1% ammonium hydroxide solution (w/v) with sonication and the monomeric peptide was confirmed by ThT, followed by dilution to 1 mL with either 50 mM tris pH 7.2 or acetate pH 5 buffer for fibril growth. Amyloid β 1−42 aliquots were fibrilized at 25 μM, while amyloid β 1−40 aliquots were fibrilized at 100 μM to start fibril growth after brief agitation. Fibrils were grown for 5 days at 37 °C and checked by ThT fluorescence to confirm fibril presence.

Cathepsin Incubations. Cathepsins were purchased from Athens Research & Technology Inc. Enzyme activity and purity were manufacturer-verified by SDS-PAGE and proteolysis of fluorescent substrates. Aliquots containing Aβ were digested by cathepsins in acetate buffer pH 5, with 1 mM ethylenediaminetetraacetic acid (EDTA) and 500 μM

https://doi.org/10.1021/acsomega.1c03915
ACS Omega 2021, 6, 31520−31527

dithiothreitol (DTT) to prevent active site oxidation. For each digestion, 0.4 μg of the enzyme was incubated with 20 μg of amyloid β for a 1:50 enzyme:substrate ratio (w/w). A control sample was set up for each digestion with no enzyme added. Incubations occurred over an 18 h period at 37 °C to allow for maximum digestion potential. Digestions were quenched by dilution with 200 mM tris before immediate fluorescent measurements.

Fluorescence Measurements. The presence of β-sheet-rich aggregates was examined by ThT assay. Samples were diluted to 2 μM in 200 mM tris buffer with 6 μM ThT. Emission scans were performed on a QuantaMaster-400 fluorimeter using an excitation wavelength of 440 nm and an emission wavelength of 485 nm.

Liquid Chromatography–Mass Spectrometry (LC–MS) Analysis. Samples were analyzed on a Thermo Fisher Ultimate 3000 RSLCnano System interfaced with a Thermo Fisher Velos Pro Orbitrap using an electrospray ionization (ESI) source. Peptides were separated on a capillary column packed in-house with C18 3 μm resin using a Shotgun Proteomics Inc high pressure vessel. Mobile phase A was water 0.1% formic acid and mobile phase B was 80% acetonitrile in water with 0.1% formic acid. Nano-ESI was performed using a spray voltage of 2.1 kV with an S-lens value of 65.

■ ASSOCIATED CONTENT

Supporting Information

The Supporting Information is available free of charge at https://pubs.acs.org/doi/10.1021/acsomega.1c03915.

Table of assignments for digests of Aβ42-acid/Aβ42-neutral digestions by catL compiled in Figure 2c, and peptide length plots for digests of Aβ42-monomeric by catL and catD with the table of assignments (PDF)

■ AUTHOR INFORMATION

Corresponding Author

Ryan R. Julian − *Department of Chemistry, University of California, Riverside, California 92521, United States;* orcid.org/0000-0003-1580-8355; Email: ryan.julian@ucr.edu

Author

Tyler R. Lambeth − *Department of Chemistry, University of California, Riverside, California 92521, United States*

Complete contact information is available at: https://pubs.acs.org/10.1021/acsomega.1c03915

Notes

The authors declare no competing financial interest.

■ ACKNOWLEDGMENTS

The authors gratefully acknowledge funding from the National Institute on Aging, R01AG066626.

■ REFERENCES

(1) Kaushik, S.; Cuervo, A. M. Proteostasis and Aging. *Nat. Med.* **2015**, *21*, 1406−1415.

(2) Mizushima, N. Autophagy: Process and Function. *Genes Dev.* **2007**, *21*, 2861−2873.

(3) Luzio, J. P.; Hackmann, Y.; Dieckmann, N. M. G.; Griffiths, G. M. The Biogenesis of Lysosomes and Lysosome-Related Organelles. *Cold Spring Harbor Perspect. Biol.* **2014**, *6*, No. a016840.

(4) Kiselyov, K.; Jennings, J. J., Jr; Rbaibi, Y.; Chu, C. T. Autophagy, Mitochondria, and Cell Death in Lysosomal Storage Diseases. *Autophagy* **2007**, *3*, 259−262.

(5) Wolfe, D. M.; Nixon, R. A. Autophagy Failure in Alzheimer's Disease and Lysosomal Storage Disorders: A Common Pathway To Neurodegeneration?. In *Autophagy of the Nervous System*; World Scientific, 2018; pp 237−257.

(6) Lambeth, T. R.; Riggs, D. L.; Talbert, L. E.; Tang, J.; Coburn, E.; Kang, A. S.; Noll, J.; Augello, C.; Ford, B. D.; Julian, R. R. Spontaneous Isomerization of Long-Lived Proteins Provides a Molecular Mechanism for the Lysosomal Failure Observed in Alzheimer's Disease. *ACS Cent. Sci.* **2019**, *5*, 1387−1395.

(7) Sharma, J.; Ronza, A. D.; Lotfi, P.; Sardiello, M. Lysosomes and Brain Health. *Annu. Rev. Neurosci.* **2018**, *41*, 255−276.

(8) Koh, J.-Y.; Kim, H. N.; Hwang, J. J.; Kim, Y.-H.; Park, S. E. Lysosomal dysfunction in proteinopathic neurodegenerative disorders: possible therapeutic roles of cAMP and zinc. *Mol. Brain* **2019**, *12*, No. 18.

(9) Bissa, B.; Beedle, A.; Govindarajan, R. Lysosomal Solute Carrier Transporters Gain Momentum in Research. *Clin. Pharmacol. Ther.* **2016**, *100*, 431−436.

(10) Turk, V.; Stoka, V.; Vasiljeva, O.; Renko, M.; Sun, T.; Turk, B.; Turk, D. Cysteine cathepsins: From structure, function and regulation to new frontiers. *Biochim. Biophys. Acta, Proteins Proteomics* **2012**, *1824*, 68−88.

(11) Turk, B.; Turk, D.; Turk, V. Lysosomal cysteine proteases: More than scavengers. *Biochim. Biophys. Acta, Protein Struct. Mol. Enzymol.* **2000**, *1477*, 98−111.

(12) Felbor, U.; Kessler, B.; Mothes, W.; Goebels, H. H.; Ploegh, H. L.; Bronson, R. T.; Olsen, B. R. Neuronal Loss and Brain Atrophy in Mice Lacking Cathepsin B and L. *Proc. Natl. Acad. Sci. U.S.A.* **2002**, *99*, 7883−7888.

(13) Koike, M. Cathepsin D Deficiency Induces Lysosomal Storage with Ceroid Lipofuscin in Mouse CNS Neurons. *Neurosci. Res.* **2000**, *38*, No. S29.

(14) Lambeth, T. R.; Dai, Z.; Zhang, Y.; Julian, R. R. A two-trick pony: Lysosomal protease cathepsin B possesses surprising ligase activity. *RSC Chem. Biol.* **2021**, *2*, 606−611.

(15) Quraishi, I.; Nägler, D. K.; Fox, T.; Sivaraman, J.; Cygler, M.; Mort, J. S.; Storer, A. C. The occluding loop in cathepsin B defines the pH dependence of inhibition by its propeptide. *Biochemistry* **1999**, *38*, 5017−5023.

(16) Kirschke, H.; Langner, J.; Wiederanders, B.; Ansorge, S.; Bohley, P.; Hanson, H. Cathepsin H: an endoaminopeptidase from rat liver lysosomes. *Acta Biol. Med. Ger.* **1977**, *36*, 185−199.

(17) Douglas Lu, W. D.; Funkelstein, L.; Toneff, T.; Reinheckel, T.; Peters, C.; Hook, V. Cathepsin H functions as an aminopeptidase in secretory vesicles for production of enkephalin and galanin peptide neurotransmitters. *J. Neurochem.* **2012**, *122*, 512−522.

(18) Ghiso, J.; Frangione, B. Amyloidosis and Alzheimer's disease. *Adv. Drug Delivery Rev.* **2002**, *54*, 1539−1551.

(19) Lam, Y. P. Y.; Wootton, C. A.; Hands-Portman, I.; Wei, J.; Chiu, C. K. C.; Romero-Canelon, I.; Lermyte, F.; Barrow, M. P.; O'Connor, P. B. Determination of the Aggregate Binding Site of Amyloid Protofibrils Using Electron Capture Dissociation Tandem Mass Spectrometry. *J. Am. Soc. Mass Spectrom.* **2020**, *31*, 267−276.

(20) Wang, H.; Shu, Q.; Rempel, D. L.; Frieden, C.; Gross, M. L. Understanding curli amyloid-protein aggregation by hydrogen-deuterium exchange and mass spectrometry. *Int. J. Mass Spectrom.* **2016**, *420*, 16−23.

(21) Ciechanover, A.; Kwon, Y. T. Degradation of misfolded proteins in neurodegenerative diseases: therapeutic targets and strategies. *Exp. Mol. Med.* **2015**, *47*, No. e147.

(22) Li, M.-Z.; Zheng, L.-J.; Shen, J.; Li, X.-Y.; Zhang, Q.; Bai, X.; Wang, Q.-S.; Ji, J.-G. SIRT1 facilitates amyloid beta peptide degradation by upregulating lysosome number in primary astrocytes. *Neural Regener. Res.* **2018**, *13*, 2005−2013.

(23) Kheterpal, I.; Williams, A.; Murphy, C.; Bledsoe, B.; Wetzel, R. Structural Features of the Aβ Amyloid Fibril Elucidated by Limited Proteolysis. *Biochemistry* **2001**, *40*, 11757−11767.
(24) Chauhan, V.; Sheikh, A. M.; Chauhan, A.; Spivack, W. D.; Fenko, M. D.; Malik, M. N. Fibrillar amyloid beta-protein inhibits the activity of high molecular weight brain protease and trypsin. *J. Alzheimer's Dis.* **2005**, *7*, 37−44.
(25) McGlinchey, R. P.; Dominah, G. A.; Lee, J. C. Taking a Bite Out of Amyloid: Mechanistic Insights into α-Synuclein Degradation by Cathepsin L. *Biochemistry* **2017**, *56*, 3881−3884.
(26) Colvin, M. T.; Silvers, R.; Ni, Q. Z.; Can, T. V.; Sergeyev, I.; Rosay, M.; Donovan, K. J.; Michael, B.; Wall, J.; Linse, S.; Griffin, R. G. Atomic Resolution Structure of Monomorphic Aβ42 Amyloid Fibrils. *J. Am. Chem. Soc.* **2016**, *138*, 9663−9674.
(27) Zhang, Y.; Rempel, D. L.; Zhang, J.; Sharma, A. K.; Mirica, L. M.; Gross, M. L. Pulsed hydrogen-deuterium exchange mass spectrometry probes conformational changes in amyloid beta (Aβ) peptide aggregation. *Proc. Natl. Acad. Sci. U.S.A.* **2013**, *110*, 14604−14609.
(28) Colletier, J.-P.; Langanowsky, A.; Landau, M.; Zhao, M.; Soriaga, A. B.; Goldschmidt, L.; Flot, D.; Cascio, D.; Sawaya, M. R.; Eisenberg, D. Molecular Basis for amyloid-β polymorphism. *Proc. Natl. Acad. Sci. U.S.A.* **2011**, *108*, 16938−16943.
(29) Fändrich, M.; Nyström, S.; Nilsson, K. P. R.; Böckmann, A.; LeVine, H., III; Hammarström, P. Amyloid fibril polymorphism: a challenge for molecular imaging and therapy. *J. Intern. Med.* **2018**, *283*, 218−237.
(30) Lu, J.-X.; Qiang, W.; Yau, W.-M.; Schwieters, C. D.; Meredith, S. C.; Tycko, R. Molecular Structure of β-Amyloid Fibrils in Alzheimer's Disease Brain Tissue. *Cell* **2013**, *154*, 1257−1268.
(31) Wälti, M. A.; Ravotti, F.; Arai, H.; Glabe, C. G.; Wall, J. S.; Böckmann, A.; Güntert, P.; Meier, B. H.; Riek, R. Atomic-resolution structure of a disease-relevant Aβ(1-42) amyloid fibril. *Proc. Natl. Acad. Sci. U.S.A.* **2016**, E4976−E4984.
(32) Colvin, M. T.; Silvers, R.; Ni, Q. Z.; Can, T. V.; Sergeyev, I.; Rosay, M.; Donovan, K. J.; Michael, B.; Wall, J.; Linse, S.; Griffin, R. G. Atomic Resolution Structure of Monomorphic Aβ42 Amyloid Fibrils. *J. Am. Chem. Soc.* **2016**, *138*, 9663−9674.
(33) Abelein, A.; Jarvet, J.; Barth, A.; Gräslund, A.; Danielsson, J. Ionic Strength Modulation of the Free Energy Landscape of Aβ40 Peptide Fibril Formation. *J. Am. Chem. Soc.* **2016**, *138*, 6893−6902.
(34) Ono, K.; Condron, M. M.; Teplox, D. B. Effects of the English (H6R) and Tottori (D7N) Familial Alzheimer Disease Mutations on Amyloid β-Protein Assembly and Toxicity. *J. Biol. Chem.* **2010**, *285*, 23186−23197.
(35) Fossati, S.; Todd, K.; Sotolongo, K.; Ghiso, J.; Rostagno, A. Differential contribution of isoaspartate post-translational modifications to the fibrillization and toxic properties of amyloid β and the Asn23 Iowa mutation. *Biochem. J.* **2013**, *456*, 347−360.
(36) Su, Y.; Chang, P.-T. Acidic pH promotes the formation of toxic fibrils from β-amyloid peptide. *Brain Res.* **2001**, *893*, 287−291.
(37) Zheng, L.; Cedazo-Minguez, A.; Hallback, M.; Jerhammar, F.; Marcusson, J.; Terman, A. Intracellular distribution of amyloid beta peptide and its relationship to the lysosomal system. *Transl. Neurodegener.* **2012**, *1*, No. 19.
(38) Shi, H.; Li, H.; Gong, W.; Gong, R.; Qian, A.; Lee, J. Y.; Guo, W. Structural and Binding Properties on Aβ Mature Fibrils Due to the Histidine Tautomeric Effect. *ACS Chem. Neurosci.* **2019**, *10*, 4612−4618.
(39) Paravastu, A. K.; Petkova, A. T.; Tycko, R. Polymorphic Fibril Formation by Residues 10-40 of the Alzheimer's ß-Amyloid Peptide. *Biophys. J.* **2006**, *90*, 4618−4629.
(40) Brännström, K.; Islam, T.; Sandblad, L.; Olofsson, A. The role of histidines in amyloid ß fibril assembly. *FEBS Lett.* **2017**, *591*, 1167−1175.
(41) Wood, S. J.; Maleeff, B.; Hart, T.; Wetzel, R. Physical, Morphological, and Functional Differences between pH 5.8 and 7.4 Aggregates of the Alzheimer's Amyloid Peptide Aβ. *J. Mol. Biol.* **1996**, *256*, 870−877.
(42) Biancalana, M.; Koide, S. Molecular Mechanism of Thioflavin-T binding to amyloid fibrils. *Biochim. Biophys. Acta, Proteins Proteomics* **2010**, *1804*, 1405−1412.
(43) Juszczyk, P.; Paraschiv, G.; Szymanska, A.; Kolodziejczyk, A. S.; Rodziewicz-Motowidlo, S.; Grzonka, Z.; Przybylski, M. Binding Epitopes and Interaction Structure of the Neuroprotective Protease Inhibitor Cystatin C with β-Amyloid Revealed by Proteolytic Excision Mass Spectrometry and Molecular Docking Simulation. *J. Med. Chem.* **2009**, *52*, 2420−2428.
(44) Schnier, P. D.; Gross, D. S.; Williams, E. R. On the Maximum Charge State and Proton Transfer Reactivity of Peptide and Protein Ions Formed by Electrospray Ionization. *J. Am. Soc. Mass Spectrom.* **1995**, *6*, 1086−1097.
(45) Shuford, C. M.; Muddiman, D. C. Capitalizing on the hydrophobic bias of electrospray ionization through chemical modification in mass spectrometry-based proteomics. *Expert Rev. Proteomics* **2011**, *8*, 317−323.
(46) Ryan, T. M.; Caine, J.; Mertens, H. D. T.; Kirby, N.; Nigro, J.; Breheney, K.; Waddington, L. J.; Streltsov, V. A.; Curtain, C.; Masters, C. L.; Roberts, B. R. Ammonium hydroxide treatment of A beta produces an aggregate free solution suitable for biophysical and cell culture characterization. *PeerJ* **2013**, *1*, No. e73.

https://doi.org/10.1021/acsomega.1c03915
ACS Omega 2021, 6, 31520−31527